Microfluidic-Assisted Interfacial Complexation of Extracellular Matrix Components to Mimic the Properties of Neural Tissues

Rui R. Costa,* David Caballero, Diana Soares da Costa, Romen Rodriguez-Trujillo, Subhas C. Kundu, Rui L. Reis, and Iva Pashkuleva*

Anisotropy is an important cue for neural organization during morphogenesis and healing, contributing to the mechanical and functional properties of neural tissues. The ability to replicate such anisotropy in vitro holds great promise for the development of effective regeneration strategies. In this work, interfacial polyelectrolyte complexation (IPC) is applied to fabricate microfibers from charged ECM components without any chemical modification. Using flow-focusing microfluidics, collagen (Col) and glycosaminoglycans (GAGs), such as chondroitin sulfate (CS) or heparin (Hep), form Col/CS and Col/Hep interfacial complexes that coalesce as IPC microfibers. These fibers are flexible and absorb large amounts of water but remain stable under physiological conditions. At these conditions, the tensile strength of the assembled Col/GAG microfibers is similar to the strength of the neural tissue. The fibers are biocompatible and biofunctional; PC12 neural cells adhere and orient longitudinally to the fibers. Moreover, Col/CS microfibers promote the formation of neural processes. The results demonstrate that the microfluidic-assisted IPC complexation enables the assembly of ECM mimics by synergetic integration of anisotropic, chemical, and mechanical cues that boost the development of neural cells.

1. Introduction

Neural tissues are composed of neurons that are responsible for communication by the propagation of electrical signals and glial cells, which protect and insulate neurons, among other functions.[1] Their extracellular matrix (ECM) is rich in collagen and sulfated glycosaminoglycans (GAGs) that account for about 20% of the adult brain volume, playing important structural and regulatory roles in cell migration, proliferation, and tissue remodeling.[2] At the microscopic level, the cellular and acellular components of the neural tissues are anisotropically organized, that is, aligned unidirectionally to guide neural/glial orientation, signal transmission, and mechanical strain. For example, white matter is made of aligned myelinated axonal fibers that deform differently when force is applied in different directions.[3]

Because neural tissues are vulnerable to trauma (e.g., sports practice, accidents) and degeneration (e.g., age- and disease-related), vital sensory and motor functions are impaired, and clinical intervention is required, commonly by implanting nerve grafts.[4] Healing can take months due to the limited capacity of neurons to regrow, and in the central nervous system, they may not regenerate at all. Novel regenerative and healing approaches recognize anisotropy as a crucial factor for efficient clinical outcomes. For example, hydrogels made of aligned fibrin fibers aid the alignment of neural cells and stimulate their

R. R. Costa, D. Caballero, D. Soares da Costa, S. C. Kundu, R. L. Reis, I. Pashkuleva
3B's Research Group
I3Bs – Research Institute on Biomaterials
Biodegradables and Biomimetics
University of Minho
Headquarters of the European Institute of Excellence on Tissue Engineering and Regenerative Medicine
AvePark
Parque de Ciência e Tecnologia
Zona Industrial da Gandra
4805-017 Barco, Guimarães, Portugal
E-mail: rui.costa@i3bs.uminho.pt; pashkuleva@i3bs.uminho.pt

R. R. Costa, D. Caballero, D. Soares da Costa, S. C. Kundu, R. L. Reis, I. Pashkuleva
ICVS/3B's
PT Government Associate Laboratory
4805-017 Braga/Guimarães, Portugal

R. Rodriguez-Trujillo
Nanobioengineering Group
Institute for Bioengineering of Catalonia (IBEC)
Barcelona Institute of Science and Technology (BIST)
Baldiri Reixac 15–21, 08028 Barcelona, Spain

R. Rodriguez-Trujillo
Department of Electronics and Biomedical Engineering
University of Barcelona
Martí i Franquès 1, 08028 Barcelona, Spain

**ADVANCED
SCIENCE NEWS**

www.advancedsciencenews.com

**ADVANCED
MATERIALS
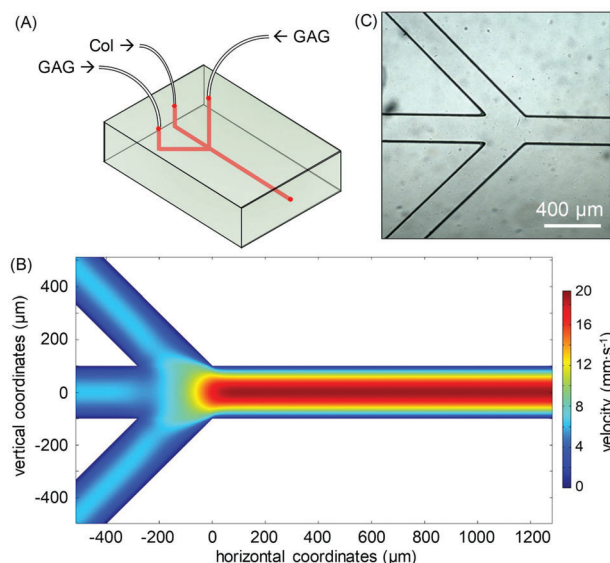TECHNOLOGIES**

www.advmattechnol.de

Figure 1. Flow-focusing microfluidic chip used to produce Col/GAG microfibers. A) 3D scheme of the chip showing the three converging microchannels and injection points for Col and GAG solutions. B) Computer simulation of fluid velocities in the microchannels. C) Micrograph of the microchip, as produced.

spontaneous electrical activity, but in contrast, hydrogels made of randomly arranged fibers induce an abnormal multidirectional signal propagation.[5] Another example showing the therapeutic benefits of anisotropic substitutes is the reduced neural cell death and mechanical stress when fibrous scaffolds from collagen[6] and polycaprolactone/carbon nanotubes[7] are used.

The gold standard for producing fibrillar structures is spinning-based fabrication. Spun constructs, for example, standalone fibers, aligned bundles, and meshes can instruct cell motility and mechanotransduction. Most traditional spinning techniques (e.g., electro- and wet-spinning) require biohazardous processing conditions, such as the use of organic solvents, high temperature or extreme pH, and are optimized for solutions of synthetic polymers,[8] excluding the use of hydrolysis-sensitive and water-soluble biopolymers. Interfacial polyelectrolyte complexation (IPC) has emerged as an alternative approach for the production of fibers under mild conditions, that is, room temperature and the use of aqueous solutions. In IPC, solutions of two oppositely charged polyelectrolytes are set in contact to establish a stable interface.[9] The fibers are drawn from the interface by pulling but not extrusion (like in other spinning techniques, for example, 3D printed aqueous two-phase systems),[10] which allows simultaneous spinning, alignment of the formed polyelectrolyte complexes, and fiber stretching. The aligned polyelectrolyte complexes establish nuclear nanofibers that coalesce into microfibers upon continuous pulling in air and drying. The obtained IPC fibers can be used as standalone constructs to direct cell adhesion and spreading[11] or as components of hydrogels for controlled drug release,[12] sutures,[13] and stem cell differentiation.[14]

There are two major challenges associated with the fabrication of IPC fibers for these applications: i) the stability of the fibers at physiological conditions/ionic strength is often compromised, which requires additional crosslinking steps to enhance the fibers' integrity; and ii) uneven distribution of the polyelectrolytes along the longitudinal fiber axis usually expressed as the formation of beads. In this work, we used a biomimetic approach to address the first challenge: we generated IPC fibers from collagen (Col) and sulfated GAGs – the most abundant polyelectrolytes participating in the ECM assembly. These biomolecules have a major role in the maintenance of ECM homeostasis and participate in downstream signaling cascades associated with specific cell responses. The used ECM components also have a structural role: they are involved in the regulation of soft tissue hydration and elasticity.[15] The complexes of Col and GAGs are stable and do not require further crosslinking or chaperones' presence, which is essential to preserve their bioactivity[16] and make this processing 'green'. To address the second challenge and optimize the processing/complexation of Col and GAGs, we amended the classical IPC processing setup by introducing a microfluidic element[17] to better control the contact between the ECM polyelectrolytes, and thus of the IPC formation and orientation in a precise and predictive manner.

2. Results and Discussion

2.1. Microfluidic-Assisted IPC Fabrication

The IPC method consists of three major steps: polyelectrolytes' contact, formation of the complexes at the interface, and complexes alignment and coalescence in the air. For the sake of comparison, we investigated if GAGs with different sulfation degrees can generate fibrillar assemblies with distinct structural properties and biofunctionality, as previously alluded to with similar compositions.[11] To this end, we used chondroitin sulfate (CS) and heparin (Hep) as polyanions.[15a] CS is abundant in perineuronal nets – ECM assemblies in the central nervous system (CNS) responsible for neural plasticity, neuroprotection, and ion homeostasis.[15b,18] Hep and its analogue heparan sulfate are also present in the ECM of CNS but in lower quantities than CS – between two to nine times less[19] – and have a different function: they regulate neurodevelopment pathways (e.g., Wnt signaling)[20] and neurotrophic factors (e.g., GDNF) involved in nerve regeneration.[15b,21] The electrostatic interactions between either of these GAGs and Col did not affect the secondary structure of the protein, as confirmed by circular dichroism (Figure S1, Supporting Information).

When processing IPC manually, fibers were formed instantly from solutions with a concentration of 3 mg mL^{-1} (Figure S2A,B, Supporting Information). However, as the complexes dried and coalesced into solid microfibers, we observed the formation of beads along the fibers (Figure S2C, Supporting Information). To overcome this drawback, we used a microfluidic device that prompts an interfacial complexation in laminar flow generated in a flow-focusing microfluidic chip with a central microchannel for Col, surrounded by two converging sheath channels for GAGs (**Figure 1**A and Figure S3, Supporting Information).

We performed an in silico experiment in which Col and GAGs were injected at a constant flow rate (5 µL min^{-1}) and obtained the parabolic profile that is typical for continuous laminar flows (Figure 1B). The microfluidic chip was then deployed while

**ADVANCED
SCIENCE NEWS**

www.advancedsciencenews.com

**ADVANCED
MATERIALS
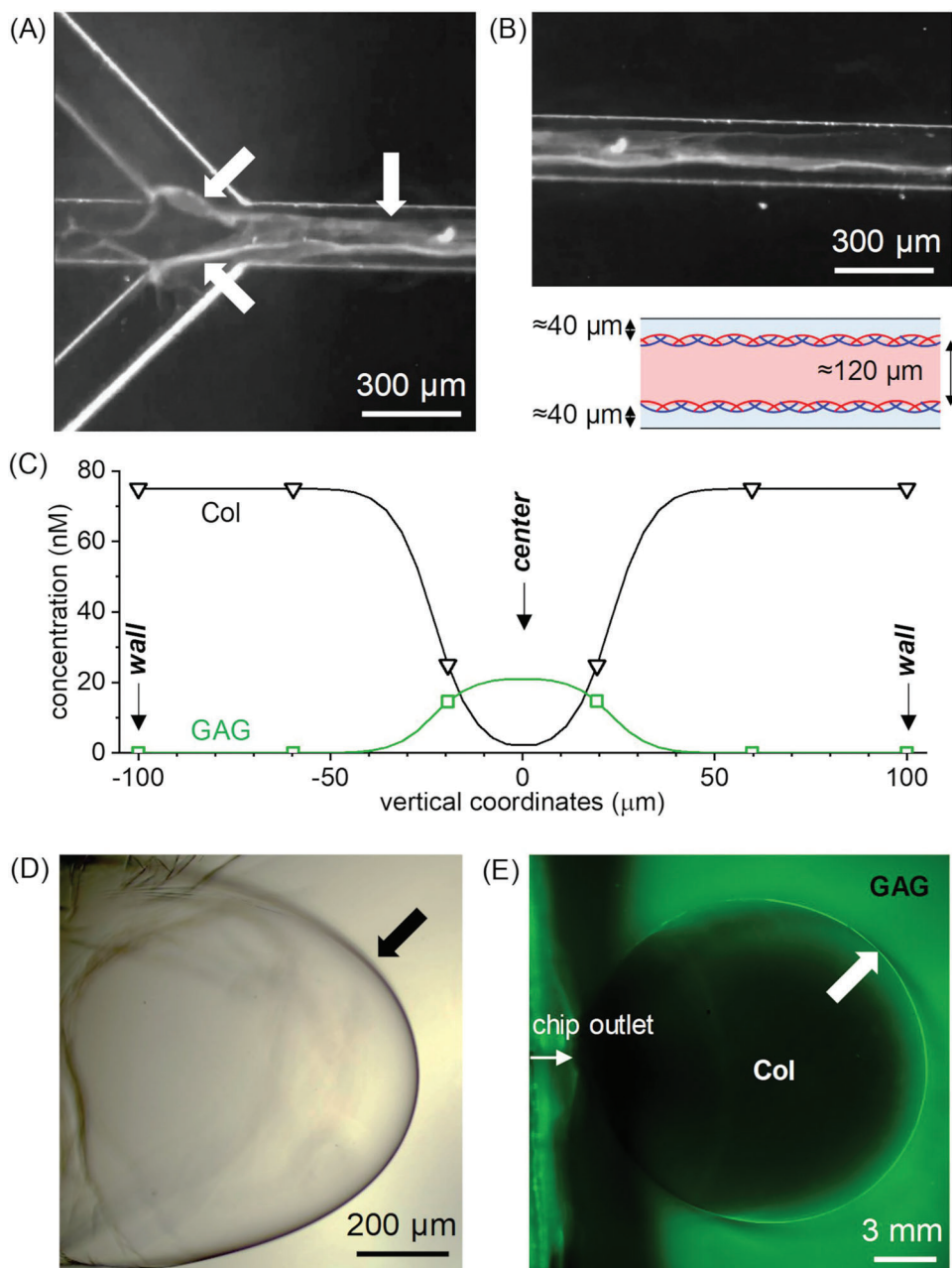TECHNOLOGIES**

www.advmattechnol.de

Figure 2. Formation of Col/GAG complex by microfluidic-assisted IPC. A,B) Darkfield microscopy images taken A) at the confluence region, and B) in the middle section of the microchannel. The white arrows point to the complex formed between the Col and GAG streams. C) Computer simulation of Col and GAG distribution in the cross-section of the central microchannel. D,E) Sac-like structures formed at the outlet of the microfluidic chip. The arrows point to the expanding interface observed under D) visible (black outline) and E) fluorescent light (green outline, enabled by using FITC-modified Hep).

maintaining the conditions used in the simulation (Figure 1C). We started by using solutions with a concentration of 5 mg mL^{-1}, aiming to achieve a high reaction yield. However, under these conditions, clotting of the microchannels by the formed complexes occurred. Therefore, we gradually decreased the concentration of the polyelectrolytes and found that a concentration of 3 mg mL^{-1} (viscosities of 11.4, 1.5, and 1.0 cP for Col, CS, and Hep, respectively) was appropriate. At these conditions, the streams of Col and GAGs stabilize instantly (4 s after injection,

Movie S1, Supporting Information) and the flow of polyelectrolytes remains constant and uninterrupted.

Upon confluence of Col and GAG streams, an albescent matter was formed (**Figure 2**A), indicating the IPC formation. This matter advanced with the flow direction and its position remained at 40–50 µm from the channel wall, as shown by the simulation data (Figure 2B,C). In a diffusive scenario, the interface would be unstable and form a diffuse gradient.[22] The stable IPC profile along the channel indicates that an interfacial complexation

between Col and GAG occurred, preventing the diffusion between streams. At the chip's outlet, a sac-like structure was formed (Figure 2D,E). The sacs had a smooth boundary and a core-shell structure with a predominant content of GAG in the shell and Col inside. As sacs grew, the interface area became thinner, indicating further the orientation of IPC due to the boundary stretch.

2.2. Col/GAG IPCs Characterization

The fibers were drawn from the sacs by manual pulling of the boundary. Different microscopies characterization showed that the proposed experimental setup enhanced the assembly process: we obtained reproducible homogeneous fibers with micro- and nano-anisotropic features (**Figure 3**), which were different from the beaded fibers assembled without microfluidic assistance. In a dry state, Col/CS and Col/Hep had average diameters of 40 and 33 µm, respectively (Figure 3A) – considerably thicker than the fibers obtained by classical IPC (average diameters of 18 and 17 µm, respectively, Figure S2C, Supporting Information). The intrinsic birefringence of the fibers allowed the use of polarized light microscopy to assess their structure: the transmission of polarized light through the specimens revealed that the Col/GAG microfibers have a crystalline structure (Figure 3B). The Col/GAG complexes aligned along the longitudinal axis, forming strands and, thus, resembling the architecture of collagenous tissues.[23] This hierarchic structure differs from the irregular structure of fibers obtained by conventional spinning techniques[24] and was achieved via the IPC orientation promoted by the laminar flow and the following pulling at the microfluidic outlet.

We used SEM to observe the surface morphology of the fibers. Both Col/CS and Col/Hep fibers exhibited surfaces with ridges along the longitudinal axis. These microstructures could be attributed to the laminar flow forces exerted during the interfacial polyelectrolyte complexation, friction effects between the flowing polymer solutions within the microfluidic chip, as well as the potential shrinking during the drying process (Figure 3C). The immunostaining of the fiber components showed the polyelectrolyte distribution (Figure 3D): in Col/CS microfibers, the polyelectrolytes were homogeneously distributed, whilst Col was predominantly found at the surface of Col/Hep microfibers, indicating the formation of a core/shell construct. This different distribution is in agreement with the anionic strength of the GAGs and its influence on the complexation process: Hep is a stronger polyelectrolyte than CS (2.7 sulfate groups per disaccharide,[25] compared to 1 in CS)[26] and forms tightly bonded complexes, while the IPC of the weaker CS retains greater molecular mobility.[27] The prevalence of Col in the shell of Col/Hep fibers can be explained by its higher molecular weight than Hep: previous studies have demonstrated that the component with the highest molecular weight resides as a support matrix of the IPC structure in the outermost regions of IPC microfibers.[11]

The IPC microfibers swelled at simulated physiological conditions (phosphate buffer, pH 7.4): fibers had diameters of 262 and 147 µm for Col/CS and Col/Hep microfibers, respectively, and the anisotropic orientation along the longitudinal axis was preserved (Figure 3E,F). Of note is the difference in the swelling de-

gree of both compositions: the volumes of Col/CS and Col/Hep fibers increased by about 40-fold and 20-fold, respectively, which is in agreement with the above-discussed polyanionic strength of the used GAGs and the lower water affinity of Hep compared to CS.[27] Besides this difference, the hydrated IPC fibers remained stable for at least 7 days and during this period, we did not observe any structural differences, that is, the core/shell structure of Col/Hep fibers was preserved (Figure S4, Supporting Information).

2.3. Mechanical Properties of the IPC Fibers

The obtained Col/GAG fibers were flexible in either dry or wet states, allowing their knitting (**Figure 4**A). This manipulation did not damage or break the fibers, that is, they were resistant and handleable. Because of the fibers' dimensions, we immobilized single strands on a paper frame (Figure 4B) to quantify the tensile strength. The measured tensile strengths of Col/CS and Col/Hep fibers in the dry state were 59 and 86 MPa, respectively (Figure 4C). In a wet state, the tensile strengths decreased dramatically: 1.6 kPa for Col/CS fibers and 10 kPa for Col/Hep microfibers, demonstrating the significant plasticizing effect of the water (Figure 4D). Of note, the strength of Col/GAG fibers was close to that of neural tissues (0.1–10 kPa),[28] making these IPC microfibers excellent candidates for neural tissue regeneration.

2.4. Culture of PC12 Neuron-Like Cells

Encouraged by the properties of the fibers obtained by the synergistic match of ECM-like composition, anisotropy, and strength of only a few Pa, we investigated the biofunctionality of the Col/GAG. For these studies, we selected PC12 cells that are derived from rat adrenal medulla and can differentiate into neuron-like cells, given their embryological origin with neuroblastic cells. Undifferentiated PC12 cells are round, but upon stimulation with the nerve growth factor NGF-β, tubulin-rich filaments are formed and extend from the round cell body. These extensions are related to neural processes and similar to neurite outgrowth.[29] The adhesion of PC12 cells to the fibers depended on the composition: more PC12 cells adhered to Col/CS fibers than to Col/Hep fibers after 7 days of culture, and the adhered cells were viable (**Figure 5**). This result indicated that the cells are sensitive to the fiber composition and that CS provided a better environment for their attachment.

Because Col is a good substrate for cell adhesion[30] and the shell of Col/Hep fibers is rich in Col, it was surprising that PC12 cells adhered less to Col/Hep fibers. The difference in the mechanical properties can explain this result: the strength of Col/Hep fibers is ≈6-fold greater than that of Col/CS fibers, placing the former composition at the upper end of the reported range for neural soft tissues. Thus, altogether the data suggests a synergism between mechano- and biochemical signaling.

Finally, we immunostained β3-tubulin to confirm the formation of neural processes in PC12 cells and evaluated their length. These processes are usually inhibited by the glial scar formation and their stimulation is critical for restoring cell-to-cell communications in injured neural tissues.[31] We used
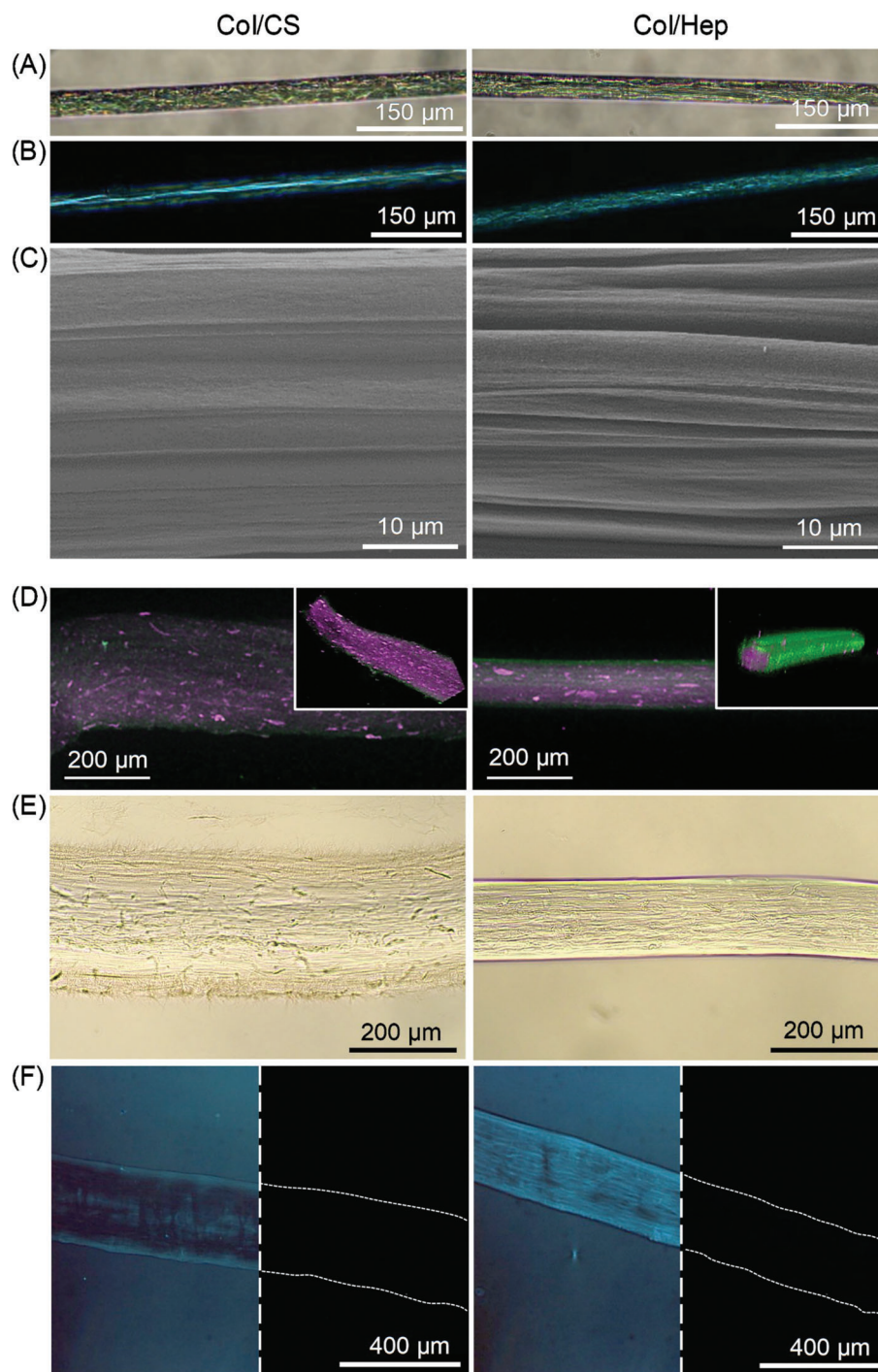
Figure 3. A–C) Micrographs of Col/CS and Col/Hep fibers in the dry state using A) brightfield, B) polarized light, and C) SEM microscopy. D) Immunostained Col/GAG fibers observed under fluorescence microscopy (purple: GAG; green: Col). Insets are 3D projections of the fibers. The luminosity of the insets was increased to improve visualization. E,F) Col/CS and Col/Hep fibers in wet state observed under E) brightfield and F) polarized light microscopy. Because the hydrated fibers contain a large amount of water, they were not visible under polarized light; the blue hue in (F) is an artifact from overlapping with the background at 100% luminosity (i.e., non-polarized light).

Col-coated tissue culture polystyrene as a control substrate to confirm the phenotype and indeed, we observed round cells with neurite-like outgrowths (Figure S5, Supporting Information). The Col/CS fibers induced the expression of β3-tubulin and the formation of long processes with an average length of 170 µm after 7 days (**Figure 6**A,B,E). Processes of PC12 on Col/Hep microfibers were less and shorter, that is, 60 µm on average (Figure 6C–E), confirming that a matrix rich in CS is essential to maintain the microenvironment of nervous tissues.
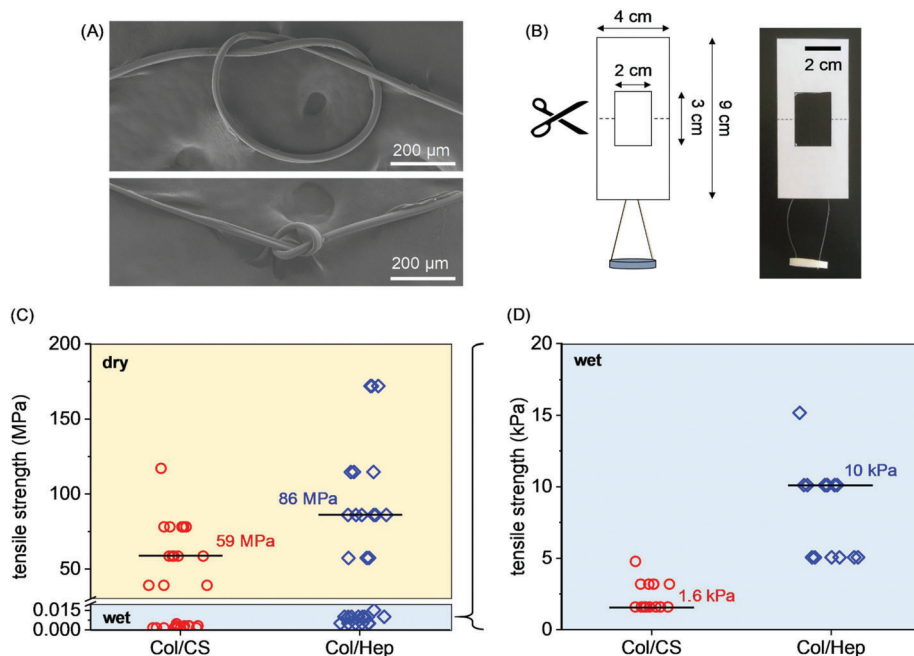
ADVANCED
SCIENCE NEWS
www.advancedsciencenews.com

ADVANCED
MATERIALS
TECHNOLOGIES
www.advmattechnol.de

Figure 4. Mechanical properties of the Col/GAG IPC fibers. A) SEM micrographs of a loose and a tight knot from Col/CS fibers shown as representative examples. B) Scheme and experimental setup used for immobilization of fibers for tensile strength measurements. C) Tensile strength data for Col/CS and Col/Hep fibers in dry and wet states. Emphasis is given to the difference in strength between the dry and the wet states. D) Tensile strength data for the hydrated fibers. The vertical axis is rescaled to kPa. The black line is the median of the respective data set.

3. Conclusion

We demonstrated that IPC of unchaperoned extracellular components, that is, collagen and glycosaminoglycans, can result in fibers that are cell instructive and stable at physiological conditions. The microfluidic assistance of the process aids the orientation of the formed IPC and ensures the formation of reproducible and homogenous fibers using a minimal quantity of bioactive polyelectrolytes. Microfluidics also allowed us to control the experimental and simulated conditions in a predictive manner.
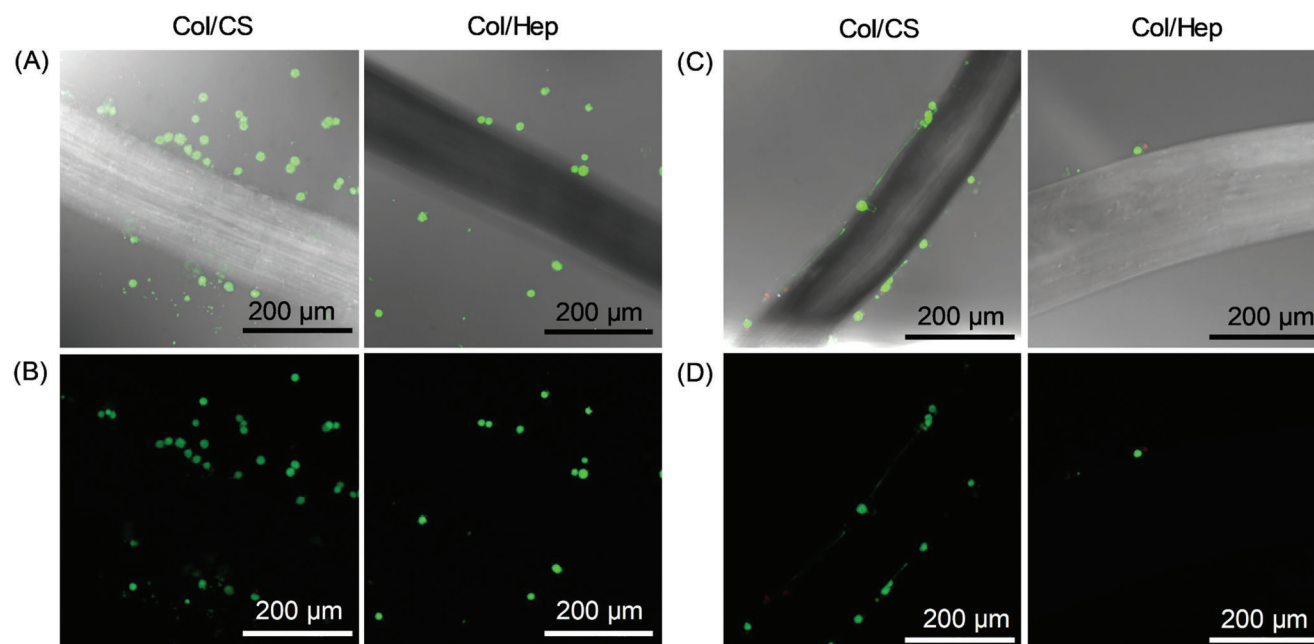

Figure 5. Live/Dead assay of PC12 neural cells adhered to the IPC fibers after A,B) 1 day and C,D) 7 days (green: live; red: dead). The micrographs depict A,C) the overlapped brightfield and fluorescence channels and B,D) the fluorescence channel alone.
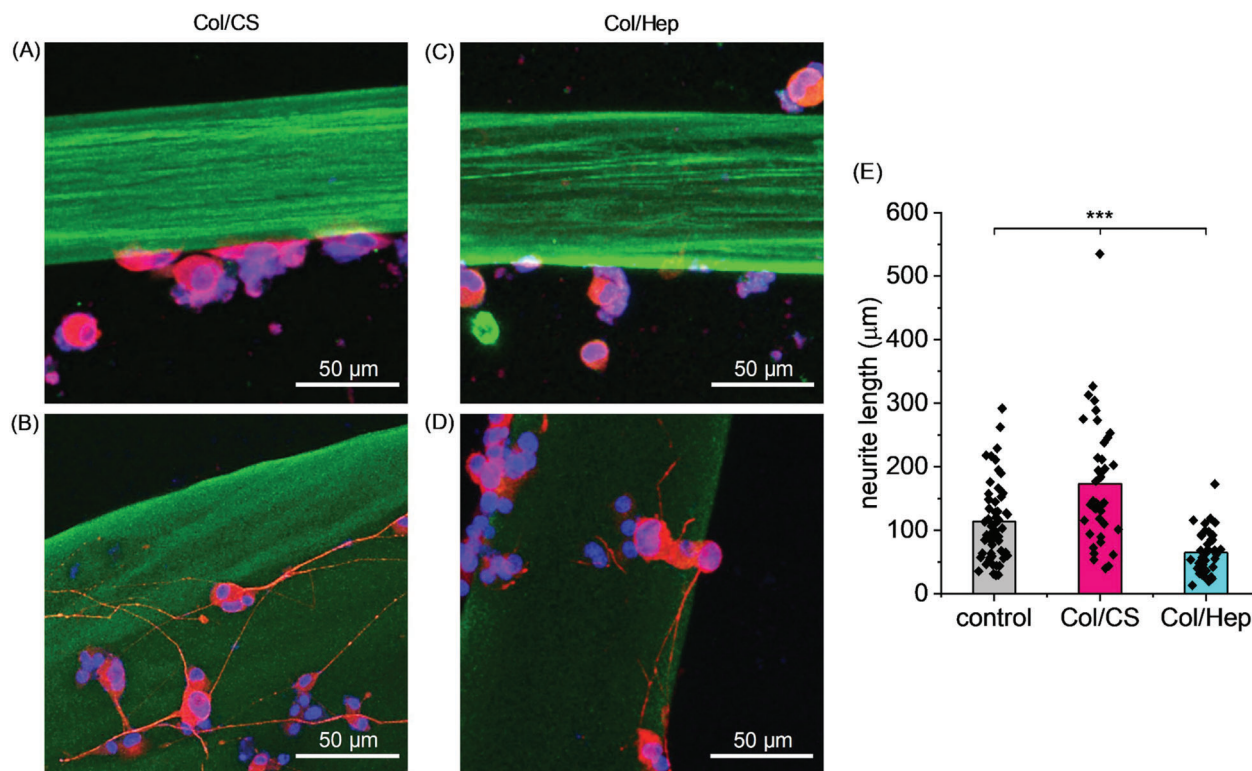
Figure 6. Representative confocal microscopy images showing PC12 cells adhered to A,B) Col/CS and C,D) Col/Hep microfibers. Culture times of A,C) 1 day and B,D) 7 days are shown. The specimens are stained for fluorescence observation (blue: nuclei; red: β3-tubulin; green: Col in microfibers). E) Length of neurite outgrowths for PC12 cells cultured on the developed IPC fibers for 7 days and control (tissue culture polystyrene coated with Col). Statistic differences ***$p < 0.001$ between all samples.

The synergy between the composition, anisotropy, and mechanical properties is important for the regeneration process, including in the observed formation of neural processes. The use of ECM components with different charges allows adjustment of the mechanical properties towards mimicking specific tissue microenvironments. The described method can be used to promote the healing and regeneration of different anisotropic tissues by tuning their composition and by including different bioactive molecules.

4. Experimental Section

Materials: Collagen type I from rat tail (Col, 139 kDa, Sigma-Aldrich), chondroitin sulfate sodium salt from shark cartilage (CS, 60 kDa, Sigma-Aldrich), and heparin sodium salt from porcine intestinal mucosa (Hep, 30 kDa, Sigma-Aldrich) were used as polyelectrolytes.

Manual IPC Spinning: Solutions of the polyelectrolytes were prepared in distilled water at 3 mg mL^{-1}. IPC fibers of Col/CS and Col/Hep were prepared by dispensing a drop (150 µL) of Col next to a drop of the respective GAG (150 µL) on a clean polystyrene surface. Polystyrene surfaces (Petri dishes 120 × 120 mm^2, Greiner Bio-One) were chosen because they are hydrophobic and prevent the drops from spreading, unlike glass (microscopy slides 25 × 75 mm^2, Deltalab) (Table S1, Supporting Information). The GAG drop was pulled towards Col one with stainless steel tweezers until they touched and after 10 s, the tweezers were pulled vertically manually at an approximate rate of 1 mm s^{-1} until a fiber of about 5 cm was obtained. The fiber ends were fixed on the Petri dish sides, leav-

ing the rest of the fiber suspended in the air. The obtained fibers were stored at room temperature for 24 h to ensure complete drying.

Finite Element Simulations: A 2D finite element method was applied to simulate the flow and diffusion of Col and GAG solutions confined into microfluidic channels. The CAD design was imported to COMSOL Multiphysics (v5.4). Col solution was injected in the central microchannel and GAG in the lateral microchannels at a fixed flow rate of 5 µL min^{-1}. Diffusion coefficients were varied in the range of typical water solutions, 10^{-10} to 10^{-9} m^2 s^{-1}. Viscosities of the Col, CS, and Hep solutions were 11.4, 1.5, and 1.0 cP, respectively, as estimated by rheology measurements (Figure S6, Supporting Information). The simulated flow and component distribution in the region immediately after the microchannels convergence ($x \geq 200$ µm) were investigated.

Microfluidic Chip Fabrication: A flow-focusing microfluidic chip containing one central and two symmetric lateral channels converging at 45° was designed by AutoCAD (AutoDesk). All microchannels were 200 µm wide and 6000 µm long (Figure S3, Supporting Information). The design was printed on an acetate photomask, which was used to fabricate a mold by conventional UV soft lithography. Briefly, negative photoresist SU8 2100 (Microchem) was spin-coated on an O$_2$ plasma-activated (30 s, 200 W) silicon wafer at 3000 rpm for 30 s to obtain a 100 µm thick layer. Next, the SU8-coated wafer was heated at 65 °C for 5 min and 95 °C for 20 min, irradiated with UV light (365 nm, 240 mJ cm^{-2}), and heated again at 65 °C and 95 °C for 5 min and 10 min, respectively. The non-crosslinked resin was removed by immersing the wafer in SU8 Developer (Microchem) for 10 min. The chip was dried with N$_2$ and left in the oven for 1 h at 70 °C to evaporate any solvent remains. Next, polydimethylsiloxane (PDMS; Sylgard 184 Dow Corning) was mixed in a 10:1 ratio (pre-polymer:crosslinker, v/v), poured on the mold, degassed, and left curing overnight at 70 °C. Once solidified, the PDMS was cut to release the lateral outlet, and the inlets were drilled with a biopsy puncher. Finally, the microfluidic chip was bonded to

a clean O_2 plasma-activated (30 s, 200 W) glass slide and stored in sterile conditions until use. The fidelity of the produced microfluidic chip to the 2D design was verified by an inverted microscope (Olympus) operating in brightfield mode.

IPC Fiber Microfluidic Processing: The operational flow rates and microchannels for Col and GAGs were fixed to the conditions used in the simulations. The solutions were injected with a multichannel syringe pump (model NE-1200, New Era Pump Systems Inc.). Experiments at higher operational flow rates – up to 15 μL min^{-1} – caused higher friction and interface instability (typical between converging fluids with large viscosity contrast),[32] which ultimately distorted the laminar flow at the junctions. The chip was placed on a polystyrene Petri dish tilted at 17° so that only the outlet touched the surface (demonstration and test of the setup in Movie S2, Supporting Information). Fibers with a length of 5 cm were pulled manually (1 mm s^{-1}) from the outlet and the ends were fixed on the Petri dish sides to dry for at least 24 h at room temperature.

Microscopy Characterizations of Col/GAG Fibers: Inverted microscopy operated in darkfield mode (Olympus) and fluorescence microscopy (Leica) were used to image the Col and GAG streams and complexation in situ. For the latter, Hep was modified with fluorescein isothiocyanate (FITC, Sigma-Aldrich), following the protocol described elsewhere.[33]

Brightfield microscopy (Olympus) was used to take micrographs of dry and wet Col/CS and Col/Hep microfibers with magnifications between 4× and 40×. Wet fibers were obtained by immersion in phosphate-buffered saline (PBS, pH 7.4, Sigma-Aldrich) for 1 h. The diameter of the fibers was measured using the Fiji image processing package (v1.53t).[34] Polarized light microscopy was performed with an Axio Observer Zeiss inverted microscope equipped with Zen software (v3.4), a 20× objective with 0.25 NA, and an Axiocam color camera (Zeiss).

Dry fibers were sputtered with gold and observed by scanning electron microscopy (SEM) using a Zeiss field emission SEM (AURIGA Compact model) with magnifications up to 2500×. The distribution of the Col and GAG in the fibers was assessed by immunostaining and confocal microscopy (Leica, TCS SP8). The fibers were stained with a collagen I monoclonal antibody (ThermoFisher, MA1-26771) followed by goat anti-mouse Alexa Fluor 594 secondary antibody and Alexa Fluor 633-conjugated wheat germ agglutinin (ThermoFisher).

Fiber Stability: The samples were immersed in Dulbecco's modified Eagle medium (DMEM, Gibco) to assess their stability. After 7 days, the samples were removed from the medium and washed with PBS. To assess the distribution of Col and GAG in the fibers, the immunostaining procedure described for the microscopy characterization of Col/GAG fibers was repeated.

Tensile Strength Measurements: The mechanical properties of dry and wet Col/CS and Col/Hep fibers were measured following an adapted ASTM D-3379 standard test method for single-filament materials. A 4×9 cm^2 paper frame with a testing window of 2×3 cm^2 at the center was used to immobilize one dry fiber specimen fixed by the extremities with super glue. Nylon wires attached a foam platform to one of the extremities of the frame. The platform was loaded with predefined weights. In the dry state, a weight of 1.5 g was first tested, followed by increments of 2.5 g. When measuring in the wet state, the fibers were hydrated in situ (PBS, pH 7.4, Sigma-Aldrich). In this case, the tested weights were 8.75 mg and multiples thereof. Fifteen specimens were tested under each condition.

Cell Culture: PC12 neural cells from the pheochromocytoma of the rat adrenal medulla were routinely cultured and expanded on collagen-coated flasks. For cell expansion, RPMI 1640 supplemented with 10% of horse serum (HS, Sigma-Aldrich), 1% antibiotic/antimycotic (ATB, Gibco), and 5% fetal bovine serum (FBS, Gibco) was used, and culture medium was replaced every 2 days. For PC12 differentiation, cells were cultured in DMEM supplemented with 1% ATB, 0.5% FBS, and NGF-β (50 ng mL^{-1}, Sigma-Aldrich) for 8 days at 37 °C with 5% CO_2 in a humidified incubator. Three sterile (UV, 30 min), 1-centimeter-long fibers were fixed on 1×1 cm^2 glass slides and seeded with differentiated PC12 cells at a density of 1×10^5 cells per sample in the presence and absence of NGF (50 ng mL^{-1}). Collagen-coated TCPS were used as controls. Samples and controls were analyzed after 1, 3, and 7 days of culture. Cell viability was determined by Live/Dead assay using calcein-AM/propidium iodide staining (Sigma-Aldrich) according to the supplier's instructions after each time point.

Immunofluorescence Analysis: PC12 cells were fixed with 10% buffered formalin for 30 min at room temperature, permeabilized with 0.2% Triton X-100 for 5 min, and blocked with 3% BSA in PBS for 30 min at room temperature. The cells were then incubated with primary antibodies against β3-tubulin (Abcam, ab18207, TUBB3) and collagen type I monoclonal antibody (ThermoFisher, MA1-26771, COLI) at 4 °C overnight (1:500 dilution), followed by incubation with a secondary antibody for 60 min at room temperature (donkey anti-rabbit Alexa Fluor 594 for TUBB3 and goat anti-mouse Alexa Fluor 488 for COLI, ThermoFisher). Cells were subsequently stained with DAPI (Biotium) for nuclei visualization.

Neurite Outgrowth Analysis: Morphometric analysis was performed on images of PC12 cells in contact with the fibers and control surfaces for 7 days. The neurite length was measured from the point of emergence at the cell body to the tip of each segment. Cells whose processes were intermingled with those of neighboring cells were excluded from the analysis. The length of the neurites was determined using the Neuroanatomy – STN plugin from the Fiji software (v.1.53t). Statistical analysis was performed by Kruskal–Wallis, followed by Dunn's multiple comparisons test.

Supporting Information

Supporting Information is available from the Wiley Online Library or from the author.

Acknowledgements

Conflict of Interest

The authors declare no conflict of interest.

Data Availability Statement

The data that support the findings of this study are available from the corresponding author upon reasonable request.

Keywords

[1] a) A. Araque, M. Navarrete, *Philos. Trans. R. Soc., B* **2010**, *365*, 2375; b) M. Wegner, C. C. Stolt, *Trends Neurosci.* **2005**, *28*, 583.

[2] C. Nicholson, E. Syková, *Trends Neurosci.* **1998**, *21*, 207.

**ADVANCED
SCIENCE NEWS**

www.advancedsciencenews.com

**ADVANCED
MATERIALS
TECHNOLOGIES**

www.advmattechnol.de

[3] Y. Feng, R. J. Okamoto, R. Namani, G. M. Genin, P. V. Bayly, *J. Mech. Behav. Biomed. Mater.* **2013**, *23*, 117.

[4] K. Kadoya, P. Lu, K. Nguyen, C. Lee-Kubli, H. Kumamaru, L. Yao, J. Knackert, G. Poplawski, J. N. Dulin, H. Strobl, Y. Takashima, J. Biane, J. Conner, S.-C. Zhang, M. H. Tuszynski, *Nat. Med.* **2016**, *22*, 479.

[5] a) Z. Zhang, M. L. Jørgensen, Z. Wang, J. Amagat, Y. Wang, Q. Li, M. Dong, M. Chen, *Biomaterials* **2020**, *253*, 120108; b) G. Zhao, Y. Feng, L. Xue, M. Cui, Q. Zhang, F. Xu, N. Peng, Z. Jiang, D. Gao, X. Zhang, *Acta Biomater.* **2022**, *139*, 190.

[6] S. H. Kim, S.-K. Im, S.-J. Oh, S. Jeong, E.-S. Yoon, C. J. Lee, N. Choi, E.-M. Hur, *Nat. Commun.* **2017**, *8*, 14346.

[7] J. Zhang, X. Zhang, C. Wang, F. Li, Z. Qiao, L. Zeng, Z. Wang, H. Liu, J. Ding, H. Yang, *Adv. Healthcare Mater.* **2021**, *10*, 2000604.

[8] a) C. S. Miranda, A. F. G. Silva, S. M. M. A. Pereira-Lima, S. P. G. Costa, N. C. Homem, H. P. Felgueiras, *Pharmaceutics* **2022**, *14*, 164; b) M. L. Siriwardane, K. DeRosa, G. Collins, B. J. Pfister, *Biofabrication* **2014**, *6*, 015012; c) J. Xue, T. Wu, Y. Dai, Y. Xia, *Chem. Rev.* **2019**, *119*, 5298.

[9] a) Q. Cui, D. J. Bell, S. B. Rauer, M. Wessling, *Adv. Mater. Interfaces* **2020**, *7*, 2000849; b) K. Ohkawa, Y. Takahashi, M. Yamada, H. Yamamoto, *Macromol. Mater. Eng.* **2001**, *286*, 168; c) M. S. Toivonen, S. Kurki-Suonio, W. Wagermaier, V. Hynninen, S. Hietala, O. Ikkala, *Biomacromolecules* **2017**, *18*, 1293; d) A. C. A. Wan, M. F. A. Cutiongco, B. C. U. Tai, M. F. Leong, H. F. Lu, E. K. F. Yim, *Mater. Today* **2016**, *19*, 437.

[10] R. C. Gonçalves, S. Vilabril, C. M. S. S. Neves, M. G. Freire, J. A. P. Coutinho, M. B. Oliveira, J. F. Mano, *Adv. Mater.* **2022**, *34*, 2200352.

[11] A. Carretero, D. Soares da Costa, R. L. Reis, I. Pashkuleva, *J. Mater. Chem. B* **2017**, *5*, 3103.

[12] M. F. A. Cutiongco, R. K. T. Choo, N. J. X. Shen, B. M. X. Chua, E. Sju, A. W. L. Choo, C. Le Visage, E. K. F. Yim, *Front. Bioeng. Biotechnol.* **2015**, *3*, 3.

[13] M. Do, B. G. Im, J. P. Park, J.-H. Jang, H. Lee, *Adv. Funct. Mater.* **2017**, *27*, 1702017.

[14] H. Zhao, J. Xu, K. Peng, X. Fu, E. Zhang, F. Lv, L. Liu, N. Zhang, Y. Wang, S. Wang, Q. Gu, *Adv. Healthcare Mater.* **2020**, *9*, 1901295.

[15] a) R. R. Costa, R. L. Reis, I. Pashkuleva, *Int. Mater. Rev.* **2022**, *67*, 765; b) D. Soares da Costa, R. L. Reis, I. Pashkuleva, *Annu. Rev. Biomed. Eng.* **2017**, *19*, 1.

[16] a) F.-M. Hsu, M.-H. Hu, Y.-S. Jiang, B.-Y. Lin, J.-J. Hu, J.-S. Jan, *Mater. Sci. Eng., C* **2020**, *112*, 110923; b) M. Li, X. Li, D. J. McClements, M. Shi, Q. Shang, X. Liu, F. Liu, *LWT* **2021**, *151*, 112121.

[17] a) M. Filippi, T. Buchner, O. Yasa, S. Weirich, R. K. Katzschmann, *Adv. Mater.* **2022**, *34*, 2108427; b) G. M. Whitesides, *Nature* **2006**, *442*, 368.

[18] S. S. Deepa, D. Carulli, C. Galtrey, K. Rhodes, J. Fukuda, T. Mikami, K. Sugahara, J. W. Fawcett, *J. Biol. Chem.* **2006**, *281*, 17789.

[19] L. Djerbal, H. Lortat-Jacob, J. C. F. Kwok, *Glycoconjugate J.* **2017**, *34*, 363.

[20] M. Colombres, J. P. Henríquez, G. F. Reig, J. Scheu, R. Calderón, A. Alvarez, E. Brandan, N. C. Inestrosa, *J. Cell. Physiol.* **2008**, *216*, 805.

[21] J. L. Roam, P. K. Nguyen, D. L. Elbert, *Biomaterials* **2014**, *35*, 6473.

[22] J. Atencia, J. Morrow, L. E. Locascio, *Lab Chip* **2009**, *9*, 2707.

[23] B. Yang, P.-Y. Lee, Y. Hua, B. Brazile, S. Waxman, F. Ji, Z. Zhu, I. A. Sigal, *J. Biophotonics* **2021**, *14*, 202000326.

[24] a) R. Dersch, T. Liu, A. K. Schaper, A. Greiner, J. H. Wendorff, *J. Polym. Sci., Part A: Polym. Chem.* **2003**, *41*, 545; b) Y. Xu, Y. Gao, X. Wang, J. Jiang, J. Hou, Q. Li, *Macromol. Mater. Eng.* **2017**, *302*, 1700054.

[25] I. Capila, R. J. Linhardt, *Angew. Chem., Int. Ed.* **2002**, *41*, 390.

[26] C. L. Haskin, G. D. Fullerton, I. L. Cameron, in *Water and the Cell* (Eds:H. Pollack, I. L. Cameron, D. N. Wheatley), Springer, Dordrecht, The Netherlands **2006**, p. 53.

[27] R. Teixeira, R. L. Reis, I. Pashkuleva, *Colloids Surf., B* **2016**, *145*, 567.

[28] a) S. Budday, G. Sommer, C. Birkl, C. Langkammer, J. Haybaeck, J. Kohnert, M. Bauer, F. Paulsen, P. Steinmann, E. Kuhl, G. A. Holzapfel, *Acta Biomater.* **2017**, *48*, 319; b) Y.-B. Lu, K. Franze, G. Seifert, C. Steinhäuser, F. Kirchhoff, H. Wolburg, J. Guck, P. Janmey, E.-Q. Wei, J. Käs, A. Reichenbach, *Proc. Natl. Acad. Sci. U. S. A.* **2006**, *103*, 17759.

[29] a) R. Hu, Q. Cao, Z. Sun, J. Chen, Q. Zheng, F. Xiao, *Int. J. Mol. Med.* **2018**, *41*, 195; b) J. Maughan, P. J. Gouveia, J. G. Gonzalez, L. M. Leahy, I. Woods, C. O'Connor, T. McGuire, J. R. Garcia, D. G. O'Shea, S. F. McComish, O. D. Kennedy, M. A. Caldwell, A. Dervan, J. N. Coleman, F. J. O'Brien, *Appl. Mater. Today* **2022**, *29*, 101629.

[30] P. Chua, W. K. Lim, *Sci. Rep.* **2021**, *11*, 8096.

[31] E. Moeendarbary, I. P. Weber, G. K. Sheridan, D. E. Koser, S. Soleman, B. Haenzi, E. J. Bradbury, J. Fawcett, K. Franze, *Nat. Commun.* **2017**, *8*, 14787.

[32] M. E. Kurdzinski, B. Gol, A. C. Hee, P. Thurgood, J. Y. Zhu, P. Petersen, A. Mitchell, K. Khoshmanesh, *Sci. Rep.* **2017**, *7*, 5945.

[33] D. S. Ferreira, A. P. Marques, R. L. Reis, H. S. Azevedo, *Biomater. Sci.* **2013**, *1*, 952.

[34] J. Schindelin, I. Arganda-Carreras, E. Frise, V. Kaynig, M. Longair, T. Pietzsch, S. Preibisch, C. Rueden, S. Saalfeld, B. Schmid, J.-Y. Tinevez, D. J. White, V. Hartenstein, K. Eliceiri, P. Tomancak, A. Cardona, *Nat. Methods* **2012**, *9*, 676.